Quantification and prediction of water uptake by soot deposited on ventilation filters during fire events

*Laura Lintis[1,2], François-Xavier Ouf[1], Philippe Parent[3], Daniel Ferry[3], Carine Laffon[3] and Cécile Vallières[2]

[1]*Institut de Radioprotection et de Sûreté Nucléaire (IRSN), PSN-RES, SCA, Gif-Sur-Yvette, 91192, France.*

[2]*Laboratoire Réactions et Génie des Procédés (LRGP), UMR 7274, CNRS - Université de Lorraine, F-54000, Nancy, France.*

[3]*CINaM, CNRS - Aix Marseille Université, F -13288, Marseille, France.*

Corresponding authors: cecile.vallieres@univ-lorraine.fr, francois-xavier.ouf@irsn.fr

Abstract

Soot samples from different fuels were produced in small and pilot combustion test benches at various O_2 concentrations, then characterized in terms of primary particle diameter, BET specific surface area and oxygen content. Water sorption measurements were then carried out for soot compacted into pellet and let in powder form, using both a gravimetric microbalance and a manometric analyzer. Water adsorption isotherms are all found of type V, and reveal the central role of the specific surface area and the oxygen content of soot. A single parametrization of the second Dubinin-Serpinsky model allows for a proper fitting of all isotherms. To our best knowledge, this is the first study to provide physicochemical parameters and water sorption results for fire soot. This enables a better description of the soot cake formed on filters during a fire, in particular in industrial confined facilities that were simulated in this study. The humidity can be then explicitly considered like other parameters influencing the aeraulic resistance of cakes. These results can contribute to better predict the consequences of fires on the containment of toxic materials within such industrial facilities.

Keywords: fire soot, physical and chemical characterization, water adsorption, Dubinin-Serpinsky model

Introduction

Need for efficient filtration devices relevant for containment of hazardous materials as nuclear materials, nanoparticles or pathogens respectively in basic nuclear installations, nanomaterials

manufacturing industry and, with regard to the SARS-CoV-2 pandemic of 2020, of biological/virological research institutes is of main importance. Beyond their initial efficiency, which is generally fixed to high level and characterized as High Efficiency Particulate Air for filters, their performance must be maintained despite hazardous situations which could eventually occur within an industrial or research confined and ventilated facilities. Furthermore, dramatic fires of the Notre-Dame Cathedral (15-16 April, 2019 in Paris, France), Lubrizol (26 September, 2019 in Rouen, France) and in contaminated surroundings of the Chernobyl site (04-05 April 2020, Chernobyl exclusion site, Ukrania) highlight the need for developing tools able to predict consequences of such fires in terms of dispersion of hazardous materials in the atmosphere [1–3]. Exposition of firefighters but also of population to such hazardous airborne transported during wildland or industrial fires is also of societal importance and open the question of performance of protective personal equipment in such accidental situation and most particularly on filtration efficiency and clogging of filtering face piece.

Soot particles, defined by Petzold et al. [4] as agglomerates of monomers consisting solely of carbon with few amounts of hydrogen and oxygen, are inevitably produced during combustion processes encountered during wildland or industrial fires. For facilities manufacturing or handling hazardous materials, soot emitted during a fire can be confined in those installations using high efficiency particulate air (HEPA) filters, but massive emission can clog those filters by formation of “cakes” [5], increasing the aeraulic resistance of the air flow passing through the filters. This enhances the mechanical strains applied on the structure of the filters, leading in extreme case to their rupture. Similar phenomena could also occur for personal protective equipment worn by firefighters or population, which could leads to an increase of the pressure drop of the filtering part, enhancing leaks and, as a consequence, decreasing the protective factor of those devices. For each of those applications and especially for safety analysis of nuclear facilities, it is crucial to be able to describe this clogging phenomenon in order to predict consequences of fires on the containment of radioactive materials. A main parameter influencing the filters clogging is the cake porosity, formed by interstitial spaces between soot aggregates. Typical porosity of soot cake has been reported above 95% [6]. Aeraulic resistance of cakes depends also on humidity [7,8], which can reach high values when water aspersion devices are used to extinguish the fire. The presence of organic vapors also influence the aeraulic resistance [5]. Thus, refined clogging models should take into account the dynamic regime of the clogging process, including high humidity variations and structural changes to which the filter and the cake are subjected to [9,10]. Furthermore, cake can be restructured in

presence of liquid water due to capillary condensation [11,12], also changing the aeraulic resistance [13]. Yet, all these phenomena have not been specifically modelled for soot emitted during a realistic fire. Indeed, due to their morphology and their potential hydrophilic character, fire soot particles can strongly adsorb water molecules leading to such capillary condensation. To develop a relevant clogging model, it is necessary to determine the water uptake of fire soot as a function of humidity and, in this context, it is particularly interesting to determine the transition between adsorption and capillary condensation. It is also relevant to understand the effect of the fire conditions (O_2 concentration, air flux) on the water uptake, as these conditions can influence the physicochemical properties of soot [14]. Water uptake measurements have been performed for chemically or thermally treated synthetic carbons, such as activated carbon [15,16], mesoporous carbon [17] and commercial carbon blacks [18,19], but have never been reported for fire soot. Carbon blacks could be considered, from a size and morphological point of view, as relevant surrogates of soot [20], but not from a chemical point of view since they are mostly composed of elemental (graphitic) carbon, while combustion soot usually denotes significant oxygen [20] and organic content [14]. Water uptake has been also measured on reference soot, emitted by laboratory burners or engines with various fuels, like diesel and kerosene [21,22]. In all cases, the main parameters influencing the water uptake are the sample porosity and the particles' chemical composition, and the main adsorption mechanism is the formation of water clusters at hydrophilic adsorption sites [23]. Numerous models for water adsorption on carbon have been proposed, especially for very porous activated carbon [24]. Among them, the Dubinin-Serpinsky (DS) adsorption model [25] is valid either for porous and non-porous carbonaceous materials. In the case of cakes of fire soot, the DS model seems relevant, as water adsorption can take place at the surface of the non-porous soot aggregates forming the cake.

Using small and pilot combustion test benches, we have produced fire soot under conditions representative of fire events [14,26]. Different O_2 concentrations of the oxidizing gas have been used to mimic the real case of a poorly ventilated and confined fire, representative of industrial facility handling hazardous materials (biological and radioactive nanoparticles). For nuclear safety application, we have considered fuels commonly found in nuclear facilities or extensively studied in the past [14]. Significant amounts of soot have been collected in order to perform physicochemical analysis and sorption measurements. TEM image analysis [27], nitrogen sorption measurements [28], elementary and XPS analysis [29] have been used to determine respectively the soot primary particles diameters, the BET specific surface area and

the global and surface oxygen contents. Water sorption measurements were carried out for soot compacted into pellet and let in powder form, using respectively a gravimetric microbalance and a manometric analyzer.

1. Experimental procedure

a. Soot production

Soot samples were produced in two cones calorimeters, one at laboratory or "lab" scale and one at "pilot" scale, differing in their dimensions, their oxidizing gas flowrates and the residence times of the emitted particles inside their combustion chamber (Figure. 1). The calorimeter at laboratory scale consists of a combustion chamber of 0.03 m^3 topped with a column in which the combustion aerosol is transported to the sampling point. We used as fuel 40 mL of heptane (Sigma-Aldrich) or DTE Medium (Exxon Mobil), a hydraulic oil used in the French nuclear industry, placed in a cylindrical container of 5.7 cm of internal diameter. We have also tested polymethyl methacrylate (PMMA), the major compound of gloveboxes walls usually used for the containment of hazardous materials (along with polycarbonate). The total flowrate of the oxidizing air was fixed at 10.8 $Nm^3.h^{-1}$, and the O_2 concentration was varied by changing the air to nitrogen ratio with two mass flow controllers (model 5853S, Brooks). We chose three O_2 concentrations of 15% (highly depleted air), 18% (depleted air) and 21% (ambient air) in the oxidizing gas for fires with heptane, DTE and PMMA. For each fuel, the soot samples are named accordingly to these oxidation conditions (*e.g.* heptane 15%, heptane 18% and heptane 21%). Soot was collected on a cellulose acetate membrane (type 11106, Sartorius Stedium Biotech) placed in a high-volume air sampler (TE-2000PX, TISCH Environmental Inc, Ohio) at a flowrate of 8 $Nm^3.h^{-1}$. In order to carry out different *ex situ* analysis, soot has been kept in a dry hermetic desiccated container, and away from light. The calorimeter at pilot scale has a significantly larger size and residence times compared to the laboratory scale ones [26]. PMMA sheets and heptane pools were used as fuels, and their respective dimensions are reported in Table 1.

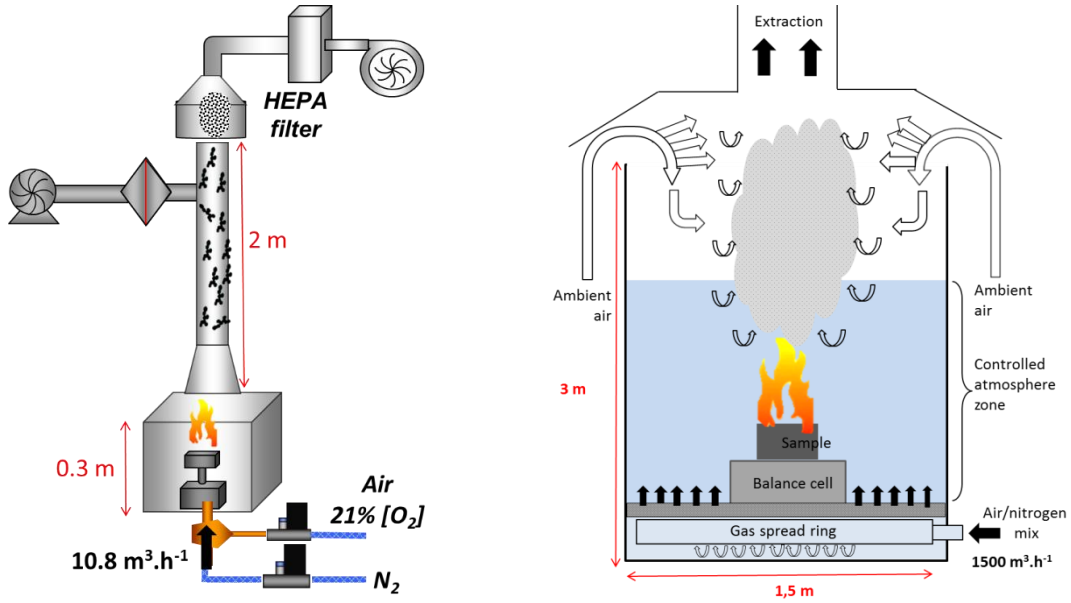

120 Figure 1: Experimental setup of the controlled atmosphere cones calorimeters at lab scale (left) and at pilot scale
121 (right)

122

123 Table 1: Summary of operational conditions for fire tests in the laboratory and pilot scale cone calorimeters

			Laboratory scale	Pilot scale
Combustion chamber volume (m^3)			0.03	22
Oxidizing gas flowrate ($Nm^3.h^{-1}$)			10.8	1500
Residence time (seconds)			10	53
Flowrate of high-volume air collector ($Nm^3.h^{-1}$)			8	60
Fuels and dimension (cm)	PMMA plate		5x5x1	40x40x3
	Liquid fuel in a cylindrical container	Heptane	∅: 5.7	∅: 21
		Hydraulic oil		

124

125

b. Physical and chemical samples analysis

The true density of the primary particles of carbonaceous aggregates was determined using a measurement technique based on the displacement of a liquid induced by the immersion of a known mass of sample. This method, described in the ISO 787-23 standard and based on the Archimedes buoyancy principle (using ethanol as displacement liquid), has been recently demonstrated to be relevant despite type of soot samples [30]. The diameters of the soot primary particles were determined by transmission electron microscopy (TEM). For TEM sampling, soot particles have been first diluted in ethanol and mixed in an ultrasonic bath during several minutes resulting to a homogeneous suspension. A microliter of this solution has been deposited on TEM grids (holey carbon film 300 mesh Cu (X25), S-147-3H from Agar Scientific®) and let drying. Soot micrographs were recorded with a Jeol 100CXII microscope equipped with a CCD camera (Gatan® Erlangshein Dualvision 300W, 780 model). A hundred of TEM images were analyzed for each sample, both manually and automatically using respectively the ImageJ software and a semi-automatic software [27]. Measurements of nitrogen sorption at 77 K using a manometric analyzer (ASAP 2020, Micromeritics) provided the specific surface area of each sample from the conventional BET analysis [31]. Prior to the measurements, the powdered samples were pumped into a primary vacuum during at least 12 hours at a temperature of 25°C. The elemental compositions of soot were determined with an organic elemental analyzer (FlashEA 1112, Thermo Scientific). Carbon, hydrogen, nitrogen and sulfur (CHNS) contents are inferred from the gas analysis emitted during a flash combustion at 920°C under oxygen. According to previous studies on carbon black samples [15,20,32], the soot oxygen content $[O]_{diff}$ (in weight %) can be determined from this analysis. In the present study, soot particles were produced from fuels mostly composed of carbon and hydrogen, and we thus expect to detect no other elements than C and H, except nitrogen and oxygen resulting from the reactions with the oxidizing gas [20,33]. The surface oxygen concentration $[O]_{XPS}$ of several soot produced at laboratory scale were determined by X-ray photoelectron spectroscopy (XPS). Prior to the XPS analysis, the samples were compacted into 7 mm diameter pellets with a hand press (Pike Technologies®). The experiments were then performed under ultra-high vacuum using a Resolve 120 hemispherical electron analyzer (PSP Vacuum) and a TX400 (PSP vacuum) unmonochromatized X-ray source (Mg Kα at 1253.6 eV) operated at 100 W. The XPS lines were deconvoluted with the CasaXPS program, using Gaussian/Lorentzian profiles and after Shirley-type background subtraction. Elemental composition is obtained from the analysis of the survey spectra and after correction by the relative sensitivity factors provided in the

program [29]. Those analytical methods have been preferred to thermo-desorption analysis of organic to elemental carbon ratio (OC/EC) since this method is not specific to surface composition and not only includes oxygen containing species but also alkyl or aliphatic groups [34] as examples.

c. Water uptake measurement

For water uptake measurements, soot samples were either in their natural powdered form, or compacted into a cylindrical pellet using a laboratory-made press functioning with a torque wrench (torque set at 0.5 N.m). Knowing the true density of soot, the global porosity (Table 2) of uncompacted ε_{powder} or compacted samples ε_{pellet} can be respectively deduced either from the volume of the powder in the cylindrical glass container, or from the diameter and the height of the pellet. Water sorption measurements were performed using gravimetric and manometric methods [35,36]. They are in good agreement whether conducted under static or dynamic sorption conditions [37,38]. Gravimetric measurements were performed only on pellets using a "dynamic vapor sorption" (DVS) Vacuum microbalance (Surface Measurements Systems, SMS). Pellets are first pumped into high vacuum during several hours at 25°C to remove water and adsorbed impurities at the sample surface. For water sorption measurements, this degassing is more recommended [39] than the conventional thermal pre-treatment that could alter surface properties, for instance by removing of hydrophilic adsorption sites. Then, the initial mass of the dried sample is determined. Subsequently, humidity steps are gradually applied at a constant water vapor flowrate. Water sweeps the sample with a limited residence time in the cell of the microbalance system, enabling to continuously renew the vapor phase in contact with the soot surface. The relative humidity RH (in %) in the microbalance is defined as the ratio between partial pressure of water $P_{H2O,vap}$ within the cell divided by the saturation pressure $P_{H2O,sat}$ (Eq. 1) at the measurements' temperature T:

$$RH = \frac{P_{H_2O,vap}}{P_{H_2O,sat}(T)} \times 100 \qquad \text{(Eq. 1)}$$

The water uptake *a(RH)* (eq. 2) is then defined as the ratio of the mass of water adsorbed ($m_{H2O,\ adsorbed}$), determined according to sample mass at each relativity humidity $m_{sample}(RH)$, and the reference mass $m_{reference}$, which is measured at RH= 0%.

$$a(RH)\frac{m_{\text{sample}}(RH) - m_{reference}}{m_{reference}} = \frac{m_{H_2O,adsorbed}(RH)}{m_{reference}} \qquad \text{(Eq. 2)}$$

The transition between two humidity steps depends on the time needed to reach the thermodynamic equilibrium and the stabilization of the sample mass with an accuracy of 0.1 µg, according to SMS. Following this value and the uncertainty propagation principle, the water uptake uncertainty is lower than 10^{-4} %. One obtains the time evolution of the mass and the maximal water uptake for a defined humidity (Figure 2) which, *in fine*, provides the sorption data needed to plot the sorption isotherms with a high accuracy. Manometric measurements were performed on uncompacted powered soot only, using a 3FLEX analyzer (MICROMERITICS). Soot samples were first degassed in a cell at 0.1 mbar and 25°C using the low vacuum pump VacPrep 061. The cell is then introduced in the 3FLEX analyzer, and water is flowed in the cell. Pressure measurements are then performed only when a stabilization criterium of 0.01 mbar.min^{-1} is reached.

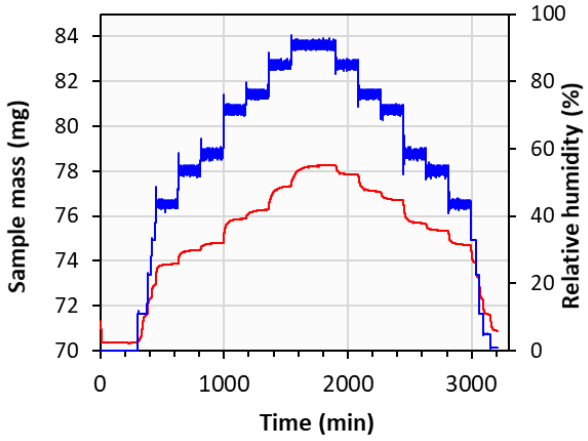

Figure 2: Example of a gravimetric measurement with the DVS microbalance (in red the evolution of sample mass and in blue the evolution of relative humidity)

d. Qualification of water uptake measurement protocol

Prior to the measurements on soot, the experimental protocols and apparatus were validated using microcrystalline cellulose (MCC) as a reference. For MCC, gravimetric, static and discontinuous sorption data are available for two kinds of samples, MCC Avicel Ph-101 provided by FMC [36] and MCC RM 302 [40], which are used as references for the COST90 standard European procedure. Figure 3 shows the water uptakes of these two MCCs following the COST90 procedure at different RH ensured by salt solutions [36], and those obtained with the DVS microbalance at the same RH steps [41]. Our results are in good agreement with the COST90 data, except slight discrepancies at high water uptakes for the MCC Avicel Ph-101. This can be explained by differences in the samples, such as size distribution or specific surface area [42]. Figure 4 compares water uptakes obtained on the MCC Avicel Ph101 at powdered

form with the 3FLEX analyzer (circles symbols) and those obtained with the gravimetric (DVS) methods (squares symbols). One can see a good agreement between the methods, as reported by previous authors [35].

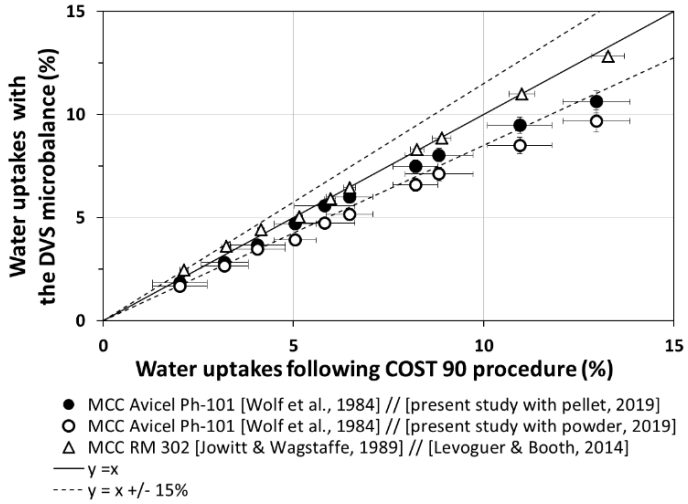

Figure 3: Comparison of water sorption data on different microcrystalline celluloses (MCC Avicel Ph-101 and RM302) obtained with the COST90 procedure and DVS microbalance

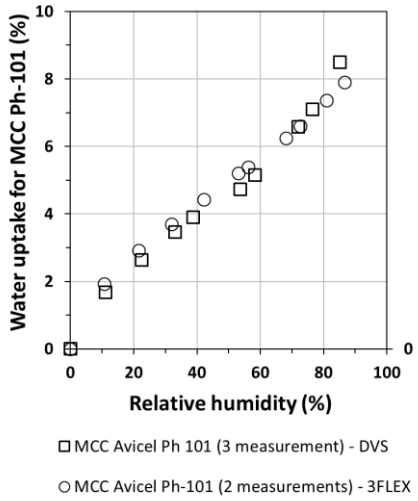

Figure 4: Water adsorption isotherms of MCC Avicel Ph-101 obtained with the DVS microbalance (squares) and with the 3FLEX analyzer (circles)

The quantities of soot being limited, experimental isotherms were generally determined once. Prior to this determination the experimental repeatability of the DVS microbalance has been checked with the MCC and two commercially available carbon black samples as size/morphological and size/morphological/chemical surrogates for this preliminary tests, respectively Printex 90 and FW200 (which denotes oxygen content close to soot particles) from Orion®. Figure 5 shows the coefficient of variation (eq. 3) for MCC Avicel Ph-101, Printex 90 and FW200 for respectively seven, five and three repeated measurements. The coefficient of

variation is lower than 10 % at water uptakes higher than 1%, indicating an excellent repeatability of the measure.

$$coefficient\ of\ variation = 100 \times \frac{standard\ deviation}{mean\ value} \quad \text{(Eq. 3)}$$

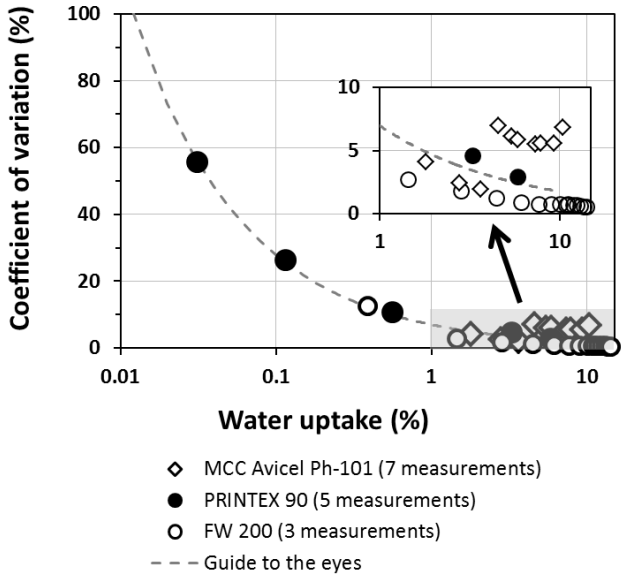

Figure 5: Repeated water sorption measurements for different samples (MCC Avicel Ph-101, PRINTEX 90 and FW200)

2. Results

a. Samples properties

The measured soot densities ρ_{true} range from 1492 kg.m^{-3} up to 1780 kg.m^{-3} (Table 2). Upper values are in good agreement with the literature for soot having a low oxygen content [43,44]. Lower density values measured for some of our samples can be explained by the presence of an organic carbon phase, which is less dense than the elemental carbon phase, reducing the overall density [30]. The diameter of the primary particles d_{pp} ranges from 22.3 nm to 43.3 nm (Table 2), in agreement with values reported for soot emitted by gaseous flames [45,46], and for more complex liquid and solid fuels [14]. For all samples, particles denote fractal morphology typical of soot particles and examples of TEM images are available in supplementary information in tables SI-1 and SI-2. Close agreement, in terms of size and morphology could then be reported between carbon black and soot samples. The specific surface area S_{BET} ranges between 52 m².g^{-1} and 100 m².g^{-1} (Table 2). This is also typical of non-porous adsorbents and agrees with values determined for soot emitted in various combustion

processes [20–22,47]. This surface area is mostly due to the surface developed by the primary particles composing soot aggregates [27]. The smaller the primary particle diameter, the higher the specific area. This explains the high surface area of PRINTEX 90 (341 $m^2.g^{-1}$), whose particles are small (25 nm) compared to FLAMMRUSS 101, whose surface area is 24.4 $m^2.g^{-1}$ because of large particles of 136 nm. We note that the S_{BET} of soot coming from hydraulic oil fire is slightly lower (53.3 to 54.2 $m^2.g^{-1}$) than the other soot produced with PMMA and heptane (75.5 to 97.9 $m^2.g^{-1}$), due to larger diameters of their primary particles. The elemental oxygen content $[O]_{diff}$ ranges between 6.4 wt. % and 11.8 wt. %, in agreement with values commonly reported in the literature [20,48]. The oxygen content is higher (up to 10 wt. %) in soot than in carbon blacks, which are known to be mostly composed of elemental carbon with oxygen concentrations lower than 2 wt. %. The oxygen concentration at the surface of the particles $[O]_{XPS}$ (Table 2) is in good agreement with the oxygen content found in the bulk $[O]_{diff}$, indicating a homogeneous repartition of oxygen within the particles.

Global porosity ε (eq. 4) has been estimated using true density ρ_{true} composing the material of soot particles, the sample mass m_{sample}, the radius r and height H of the cylindrical soot pellet or of the glass container for the uncompacted samples. For soot pellets, the global porosity ε_{pellet} ranges between 29% and 66%. This wide range of values probably results from different adhesion properties of each sample during the compaction process. The global porosity of the powdered soot samples ε_{powder} is around 96% for all samples, close to typical soot cake porosities reported on HEPA filter [6].

$$\varepsilon = 1 - \frac{m_{sample}}{\pi r^2 H \rho_{true}} \qquad \text{(Eq.4)}$$

b. Water isotherms of soot particles produced under different fire conditions

Fig. 6 presents the gravimetric water adsorption isotherms for soot compacted into pellets. The water uptakes are obtained considering a reference mass $m_{reference}$ as the mass of sample at RH=0%. Overall, all the samples present the same slopes and the water uptakes range from 2.4% and 3.6% (at RH=90%). This results from similar physicochemical properties of all soot in terms of structure and composition. From RH= 0% to 80%, the isotherms are of V^{th} type according to the IUPAC classification [49]. They present a rather slight convex curvature at RH < 30%. On the isotherms, this convexity combined with a positive slope is characteristic of low

Table 2: Summary of the physicochemical properties of soot and carbon black samples studied

Samples	ρ_{true} ($kg.m^{-3}$)	d_{pp} (nm)	S_{BET} ($m^2.g^{-1}$)	$[O]_{diff}$ (wt.%)	$[O]_{XPS}$ (wt.%)	ε_{pellet} (%)	ε_{powder} (%)
Soot							
Heptane 21% (lab scale)	1780±20[1]	35.1±1.3	75.5±0.7	7.6±0.8	7.4	62±3	96±1
Heptane 15% (lab scale)		22.8±0.5	97.9±2.3	11.8±1.2	8.8	54±4	
PMMA 21% (lab scale)	1492±12[1]	39.9±0.8	79.3±1.1	6.7±4.8	9.9	54±4	
PMMA 18% (lab scale)		32.2±0.8	84.4±1.2	9.2±0.6	8.1	29±7	
DTE Medium oil 21% (lab scale)	1593±336	42.1±1.2	53.3±1.1	9.2	8.8	58±10	
DTE Medium oil 18% (lab scale)		38.6±1.1	54.2±1.2	9.9±0.4	9	56±10	
Heptane 21% (pilot scale)	1780±20[1]	34.1±1.3	69.5±0.7	6.8±0.8	n.d.	66±3	
Heptane 15% (pilot scale)		29.9±0.9	86.9±1.2	9.1±0.6		58±4	
PMMA 21% (pilot scale)	1492±12[1]	35.9±1.1	69.2±1.4	6.4±0.8		59±4	
PMMA 18% (pilot scale)		37.2±1.2	63.7±1.4	7.1±1.8		52±4	
Carbon blacks							
PRINTEX 90	1783±45	25±1	340.0±1.6	1.1		62±5	88±2
FLAMMRUS 101	1712±85	136±8	24.4±0.1	2.1		71±4	78±3
COLOUR BLACK FW200	1800[2]	21±2	506±2.0	18.6±0.2	n.d.	54±1	-

[1] From [30]

[2] From manufacturer

interactions of water at the surface, with locally high interaction with some hydrophilic adsorption sites of the soot surface [50]. A slight inflexion point is observed at RH=80% for the heptane 15% soot obtained at pilot scale (Figure 6 left, red triangles), revealing the beginning of capillary condensation.

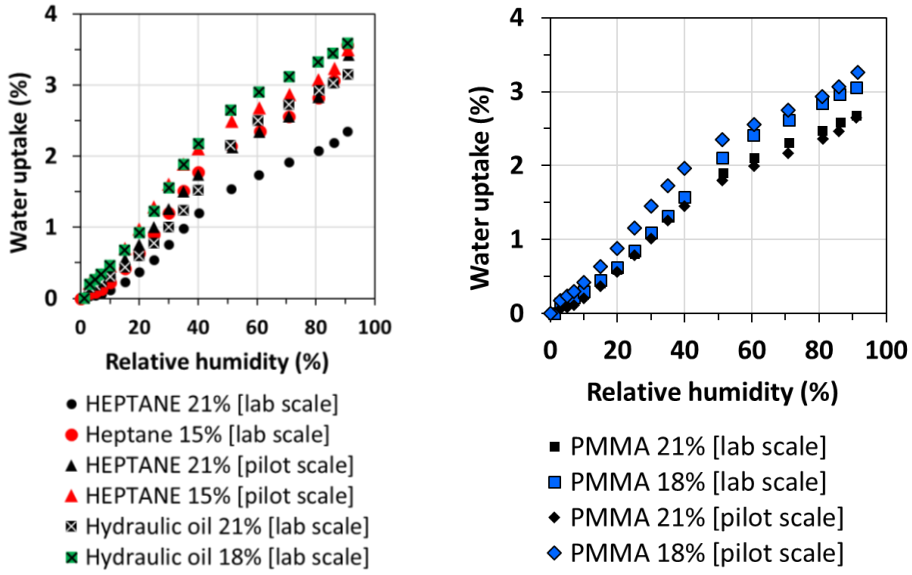

Figure 6: Water adsorption isotherms for soot produced with liquid fuels (left) and PMMA (right)

The water uptakes measured on the DTE hydraulic oil soot samples are slightly higher than for the heptane and PMMA soot samples. Figure 7 compares the water uptakes obtained on fire soot samples produced at laboratory scale and at pilot scale. Except for the heptane soot produced at 21% of O_2 concentration, water uptakes are globally similar whatever the scale, with a maximal difference of ±15%. For the considered fuels, fire scale has no major influence on the water adsorbing properties.

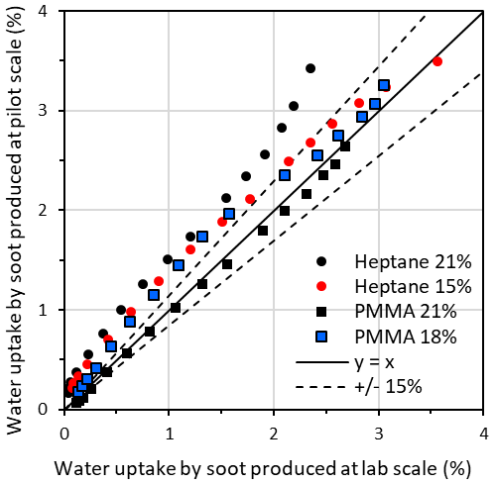

Figure 7: Comparison between water uptakes of soot samples produced at pilot and laboratory scale

Figure 8 compares the water uptakes on soot produced at 21% of O_2 concentration (ambient air value) with those produced at depleted O_2 concentrations (15%, 17% and 18 %), which adsorb up to 50% more water than soot produced at ambient concentration (see Figure SI-1 in supplementary information). This highlights the significant modification of size (decrease of primary particle size and increase of specific surface area) and composition (increase of oxygen content) of soot particles with decreasing oxygen concentration reported in Table 2 and in agreement with previous findings [14,51]

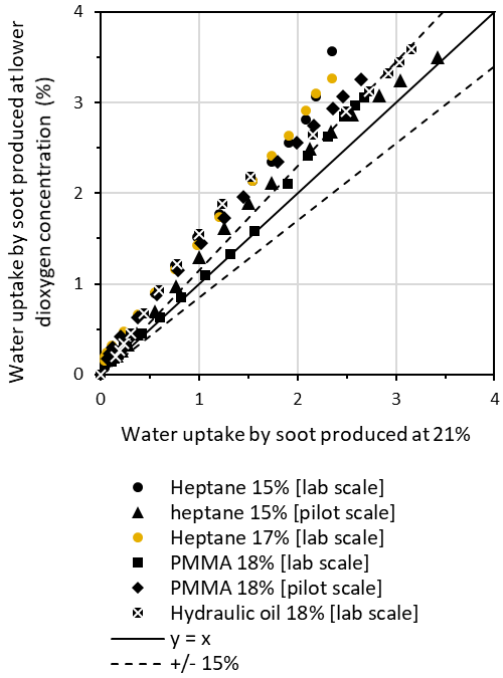

Figure 8: Comparison between water uptakes obtained for soot samples produced at depleted oxygen concentrations (15-18%) and ambient oxygen concentration (21%)

c. Influence of specific surface area and oxygen surface content of water uptake

Figure 9 presents the water uptakes obtained at the maximal RH of 90% as a function of the specific surface area, for all fire soot samples and for PRINTEX 90 and FLAMMRUSS 101. These carbon black samples are mostly composed of elemental carbon. Their water adsorption isotherms are of type III (see supplementary information, Figure SI-2), which indicates low carbon black-water interactions and a water uptake related to the specific surface area only. Additional data on carbon black samples available in the literature - whose compositions are globally similar to our samples - are also plotted in Fig. 10 (identified with an asterisk "*" [18,19,21,52]). Over the whole specific surface area range, soot particles present higher water uptakes than carbon blacks and do not follow the linear correlation proposed on

312 Fig.10. Those discrepancies between soot and carbon blacks can be explained, beyond the
313 geometric surface associated to the cake structure, by their specific chemical composition.

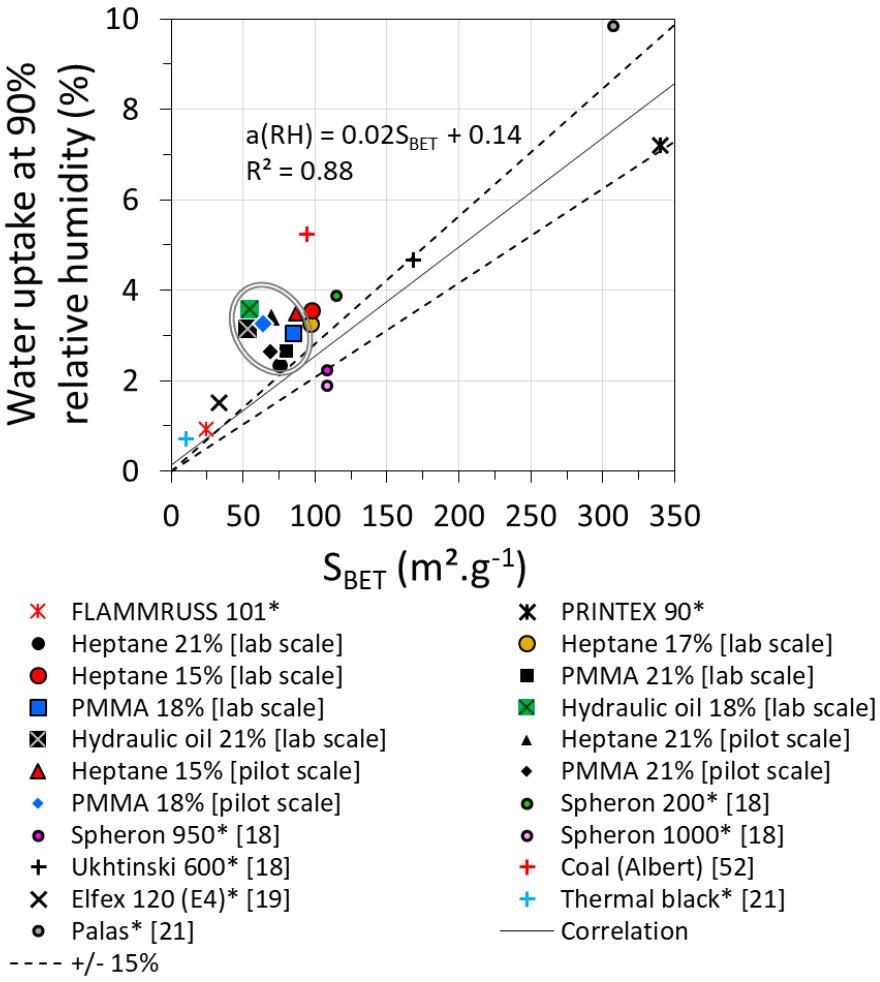

314

315 Figure 9: Effect of specific surface area on water uptake at 90% of relative humidity

316 To assess the influence of the sample composition on the water sorption capacity, water
317 uptake can be expressed as the number of water statistical monolayers (ML) needed to cover
318 entirely the sample surface (Eq. 5). This unravels the effect of the surface area from the
319 chemical composition:

320 $$ML = \frac{(a(mmol.g^{-1})\times 10^{-3})\times N_A(mol^{-1})}{\frac{S_{BET}(m^2.g^{-1})}{\sigma_{H_2O}(m^2)}} \quad \text{(Eq. 5)}$$

321 Where σ_{H2O} is the surface occupied by a water molecule ($1.05.10^{-19}$ m²), a the amount of
322 adsorbed water per mass of sample, N_A the Avogadro number ($6.022.10^{23}$ mol^{-1}) and S_{BET} the
323 specific surface area (m².g^{-1}).

Figure 10 shows the evolution of ML with the surface concentration of oxygen $[O]_{surface}$, calculated as the mass of oxygen per surface area (Eq. 6).

$$[O]_{surface}\ (g.m^{-2}) = \frac{[O]_{diff}(wt.\%)}{100.S_{BET}(m^2.g^{-1})} \qquad \text{(Eq. 6)}$$

The oxygen content is known to significantly influence the water sorption [23]. The oxygenated chemical functions located at the surface strongly interact with water molecules, especially in the range of low humidity where they represent the energetically most favorable adsorption sites [50]. To highlight this effect, we have plotted ML at RH= 30% and RH= 90 % (left and right sides on Fig. 10 respectively) as a function of $[O]_{surface}$ for all our samples and those available in the literature. ML linearly increases with $[O]_{surface}$ with a slope of 5.33 (RH=30%) and 13.57 (RH=90 %). This clearly shows that the oxygen concentration at the surface significantly enhances the adsorption process, with a similar physico-chemical mechanism within relative humidity range 30-90 % (as a same linear dependence is observed at RH= 30 % and 90 %).

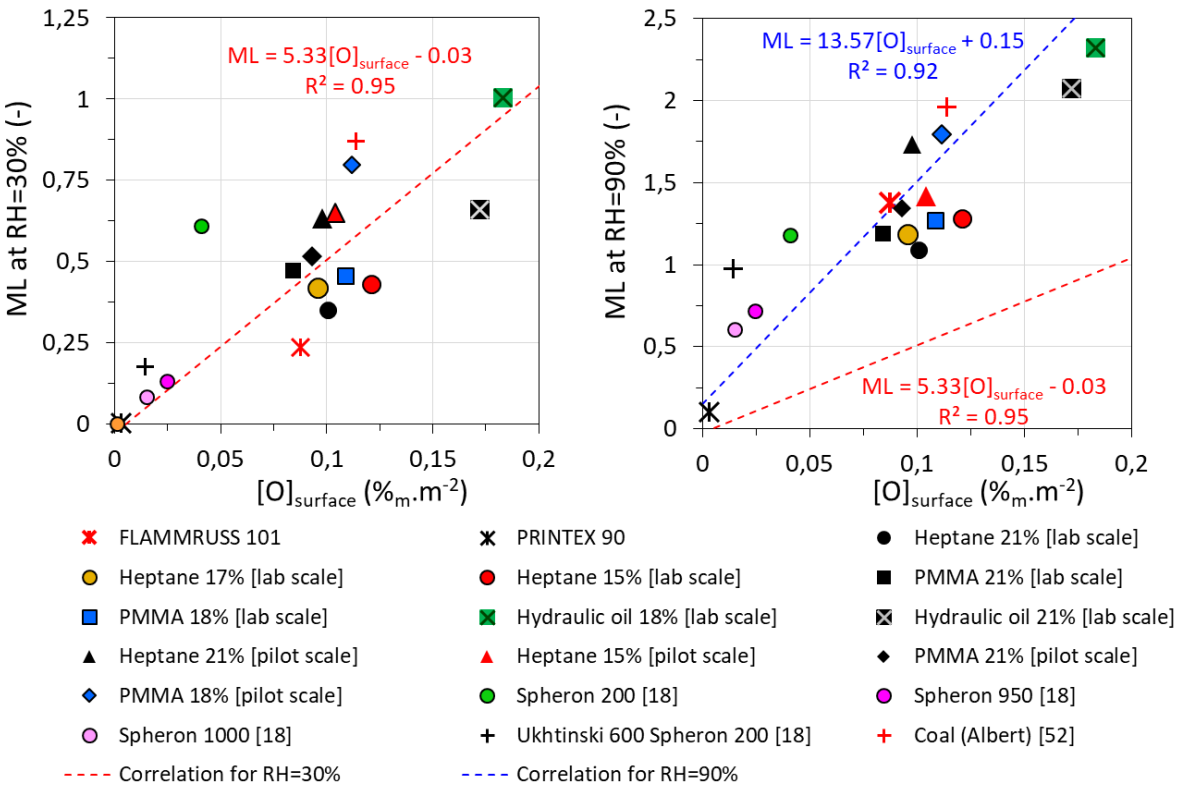

Figure 10: Evolution of the number of ML with the surface concentration of oxygen, at RH = 30% (left) and RH = 90% (right)

Figure 11 compares, for each relative humidity step (+/- 1%), the water uptakes obtained for the pellets with the DVS microbalance and for the powders with the 3FLEX analyzer (the

corresponding water adsorption isotherms are available for 3FLEX as supplementary information, Fig. SI-3). This figure shows that water uptakes for powder and compacted samples are globally equivalent in a +/- 15% interval. However, exceptions can be observed for heptane 15%, heptane 21% and PMMA 21% [pilot scale], where adsorption is higher for powder than for pellet, especially at high water uptake (related to higher relative humidity). This could be explained by different mesostructures of these soot samples when they are characterized in pellet or in powder forms, changing the surface and volume available for water adsorption.

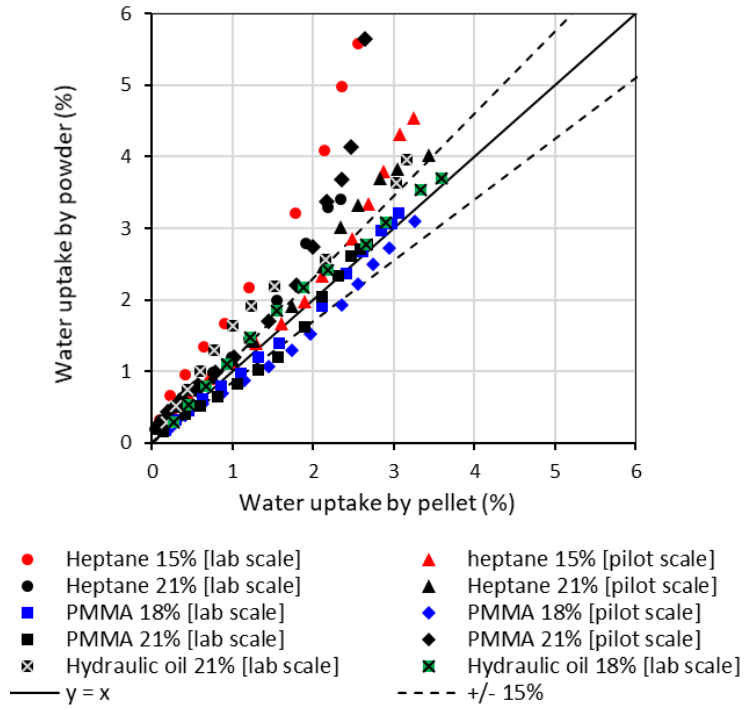

Figure 11: Parity diagram comparing the water uptakes between pellets and powders at different humidity steps

4. Discussion

Until now, the water sorption on carbon systems have been mostly modelled for activated carbon or carbon/zeolite [53] whose isotherms are systematically of V^{th} type. Several common water sorption models have been established for such isotherms, considering a primary adsorption on specific hydrophilic surface sites followed by adsorption on already adsorbed water molecules. This second adsorption process is driven by water-water interactions, which are, overall, more favorable than those between water and a globally hydrophobic carbonaceous surface. Being an associating fluid, water can finally fill in the micro-and-mesoporous pore volume. Unlike activated carbon, soot particles are made of non-porous hydrophobic carbon,

porosity being only due to interstitial spaces between the primary particles in the soot cakes, which also varies with the sample conformation (powder or pellet). The surface of soot is mostly hydrophobic, with some hydrophilic adsorption sites related to the presence of surface oxygen. As previously mentioned, one of the most suitable sorption model for such porous solid is the Dubinin-Serpinsky (DS) one [54,55]. This model describes a mechanism of water clusters formation on the adsorbent surface sites, which can be followed by a pore volume filling [56,57]. In the DS model, the adsorption process is considered as an equilibrium state of a chemical reaction between water molecules in the gaseous phase H_2O_{gas} and the adsorption sites located on the adsorbent surface $S_{adsorbent}$ (Figure 12). Those sites can be primary or secondary, corresponding respectively to the initial number of hydrophilic sites a_0 (%g.g$^{-1}_{adsorbent}$) and the already adsorbed water molecules a per gram of sample (expressed here in terms of %g.g$^{-1}_{adsorbent}$). This equilibrium is formalized by the equilibrium constant c (defined as the ratio between kinetic constants associated to adsorption k_{ads} and desorption k_{des}), enabling to express a, the total amount of adsorbed water (Eq. 7), including the water vapor relative pressure h.

$$c = \frac{k_{ads}}{k_{des}} = \frac{a}{h a_0} \qquad \text{(Eq. 7)}$$

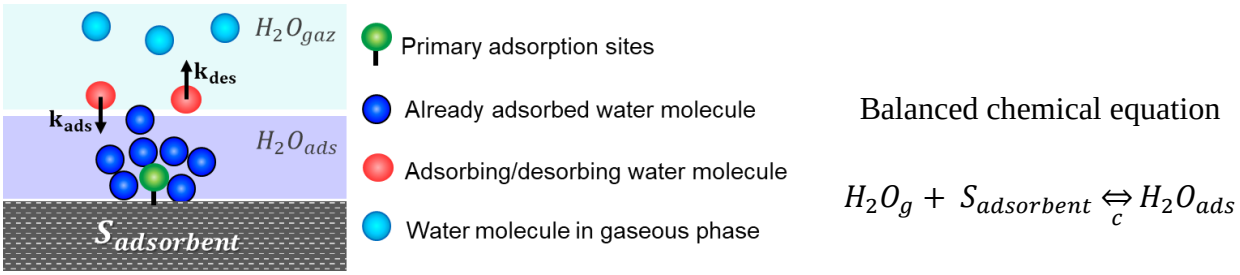

Figure 12: Scheme of the proposed mechanism of water adsorption and formula used to express the Dubinin-Serpinsky model

Among all the DS model versions [24], the second version, commonly called DS2, has the simplest analytical form and takes into account the limitation of adsorption with the water uptake due to the steric hindrance. To this aim, a dimensionless and strictly positive factor *(1-ka)*, decreasing with the adsorbed water amount, has been added to the original DS equation (Eq. 8). The constant k has therefore a value that ranges from 0 to strictly inferior to $1/a$. This constant corresponds to the proportion of water molecules which does not act anymore as a secondary adsorption site (steric hindrance). It leads to the analytical form of 2nd version of DS model (eq. 8).

$$a = c(a_0 + a)h(1 - ka) \quad \text{(Eq. 8)}$$

Where *k* is the coefficient related to the steric hindrance due to the formation of water clusters ($\%g_{adsorbent}.g^{-1}$).The adsorption isotherms obtained in the present study have all been successfully fitted with the DS2 model in the relative humidity range of 0%-90% (Fig. SI-4). Fitted parameters k, a_0 and c for all samples are also available in Table SI-3, with regression coefficients R^2 all above 0.99. This indicates a unique adsorption process consisting in the formation of water clusters on few hydrophilic sites, which we assume to occur on the oxidized surface sites.

The fitted values of *k* are 0.24 ± 0.02 and 0.14 ± 0.03 for pellets and powders, respectively. The higher *k* value for pellets is a consequence of a limited secondary adsorption process, indicating a higher steric hindrance to clusters formation compared to powders. This is likely due to the higher compaction of the pellets, which facilitates the blocking of interstitial spaces between the soot particles. Decrease of *k* values is consistent with the increase of mean concentrations of primary adsorption sites a_0 (in $\%g.g^{-1}_{adsorbent}$), from 1.0% ± 0.4% for pellets to 2.6% ± 0.4% for powders. The lower value of a_0 for pellets indicates a lower accessibility to the adsorption sites by the filling of the pores where the primary adsorption sites are located, while more sites are available in powders. The mean values of equilibrium constant *c*, corresponding to the ratio of the kinetic constants between adsorption and desorption processes, are 2.6 ± 0.4 and 1.6 ± 0.4 for the pellets and powders respectively. Taking into account their uncertainties, these values remain quite close and, at this stage, we cannot explain such a slight difference in the kinetic constant without any further investigations.

As previously reported in the literature [6], porosity of soot cake formed at HEPA filters surface are generally between those considered in the present study for pellets (mostly 50-60%) and powder (95%). To provide useable values of *k*, a_0 and *c* that could be implemented in clogging models for similar kinds of hydrophobic soot [5,58], we have averaged the fitting parameters *k*, a_0 and *c* of the 22 studied samples, whether compacted into pellet or not. These values are reported in Table 3, along with their standard deviation. Figure 13 presents the computed water uptakes using these averaged values and deviations plotted against the experimental water uptakes for all soot samples. We observe that 95% of the water uptakes (limited in the present case to water uptake values higher than 1%) can be satisfactorily represented by the DS2 model using these averaged parameters, within a confidence interval of ± 47%.

Table 3: Calculated values from 22 water adsorption isotherms

	k (%)	a_0 $(\%g.g_{adsorbent}^{-1})$	c (-)
Mean value	0.20	1.54	2.23
Standard deviation	0.056	0.85	0.69
Expanded uncertainty for a 95% confidence interval	0.012	0.18	0.15

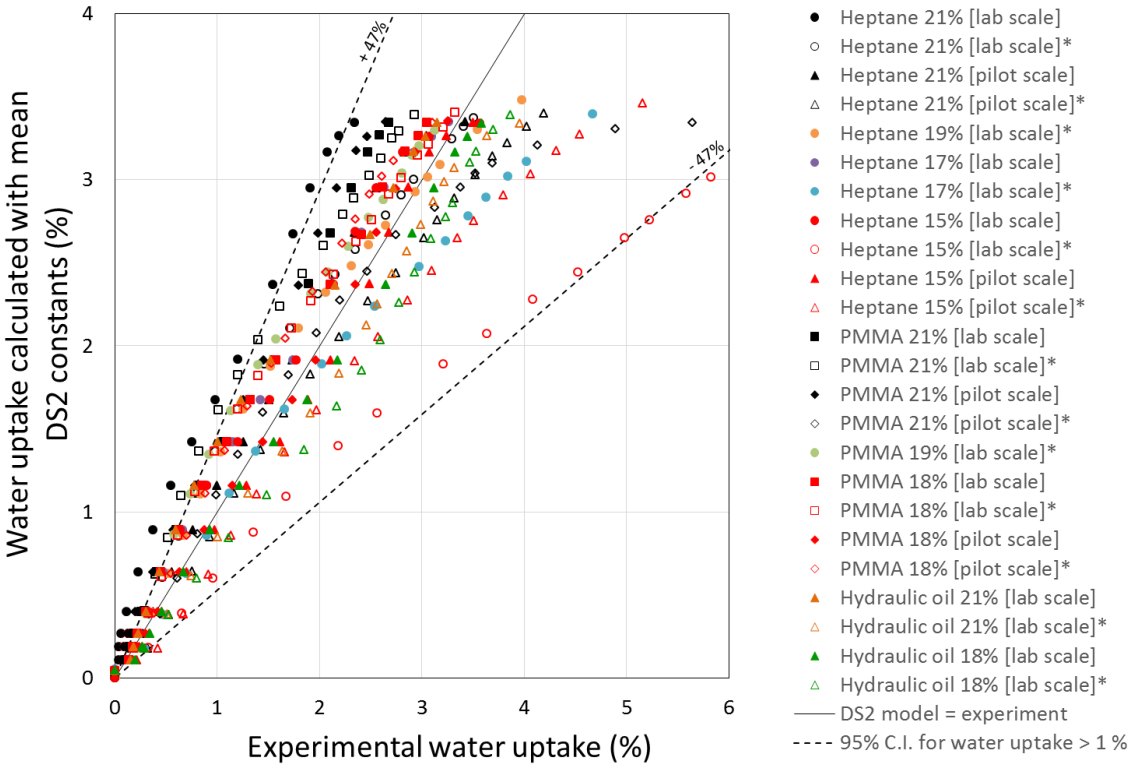

Figure 13: Comparison between DS2 model, computed according to mean constants, and experimental water uptakes

5. Conclusion

This study aimed at measuring the water uptake in soot cakes representative of those formed on HEPA filters during fire occurring in a nuclear plant. For this purpose, soot was produced at laboratory and pilot scales with different fuels - heptane, PMMA and hydraulic oil- representative of fuels encountered in a real nuclear plant. The physicochemical properties of these samples have been determined *ex situ* with analytical techniques providing the specific

surface area, the primary particle diameters and the oxygen contents, found respectively in the ranges of 52 $m^2.g^{-1}$ – 100 $m^2.g^{-1}$, 22.3 nm – 43.3 nm and 6.7wt. % - 9.9 wt. %. We have shown that these physicochemical properties are only slightly influenced by the fire scale, the fuel type, or the O_2 concentration of the oxidizing gas. Using gravimetric and manometric techniques, we have measured the water uptake of these samples as well as two additional carbon black samples, let in powder form or compacted into pellets. Gravimetic and manometric approaches have been proven equivalent, with a variation coefficient lower than 10% for the whole relative humidity range (0%-100%). The adsorption isotherms of soot are of V^{th} type and present maximal water uptakes between 2% and 4% at RH=90%. Under the investigated conditions, fire scale does not significantly impact the isotherms classification. Two physicochemical properties of soot directly impact the sorption process: the specific surface area and the oxygen concentration per surface area. The very good fit of the experimental isotherms with the second Dubinin-Serpinsky model (DS2) indicates that adsorption occurs by nucleation of water clusters on few oxidized and hydrophilic surface sites. The DS2 parameters have been obtained for the 22 studied samples, either compacted or as powders, and their average allows for a proper simulation of 95% of the experimental data. This model will contribute to the improvement of simulation codes and consequently to better predict the HEPA filter clogging phenomenon during a fire in nuclear facility. In addition, the use of the second Dubinin-Serpinsky model appears relevant to represent the water sorption isotherms of fire soot.

Acknowledgements

The authors would like to thank Guillaume Basso, Mickael Coutin, Vincent Cozar, Hugues Pretrel, Serge Pons and Pascal Zavaleta from the “Laboratoire d’Expérimentation des Feux” in Cadarache for providing soot samples emitted during large-scale fire experiments. This work was partially done within the framework of the LIMA joint research program (The Interactions Media-Aerosol Laboratory) between the Institut de Radioprotection et de Sûreté Nucléaire (IRSN) and the Reactions and Chemical Engineering Laboratory (LRGP) of the French National Centre for Scientific Research (CNRS).

References

[1] F.-X. Ouf, T. Gelain, M. Patry, F. Salm, Airborne release of hazardous micron-sized metallic/metal oxide particles during thermal degradation of polycarbonate surfaces contaminated by particles: Towards a phenomenological description, J. Hazard. Mater. 384 (2020) 121490. https://doi.org/10.1016/j.jhazmat.2019.121490.

[2] L. Howes, Lead contamination risk near Notre-Dame cathedral, Chem. Eng. News. 97 (2019) 6–6. https://doi.org/10.1021/cen-09718-scicon3.

[3] N. Evangeliou, S. Zibtsev, V. Myroniuk, M. Zhurba, T. Hamburger, A. Stohl, Y. Balkanski, R. Paugam, T.A. Mousseau, A.P. Møller, S.I. Kireev, Resuspension and atmospheric transport of radionuclides due to wildfires near the Chernobyl Nuclear Power Plant in 2015: An impact assessment, Sci. Rep. 6 (2016) 26062. https://doi.org/10.1038/srep26062.

[4] A. Petzold, J.A. Ogren, M. Fiebig, P. Laj, S.M. Li, U. Baltensperger, T. Holzer-Popp, S. Kinne, G. Pappalardo, N. Sugimoto, C. Wehrli, A. Wiedensohler, X.Y. Zhang, Recommendations for reporting black carbon measurements, Atmos. Chem. Phys. 13 (2013) 8365–8379. https://doi.org/10.5194/acp-13-8365-2013.

[5] V.M. Mocho, F.X. Ouf, Clogging of industrial pleated high efficiency particulate air (HEPA) filters in the event of fire, Nucl. Eng. Des. 241 (2011) 1785–1794. https://doi.org/10.1016/j.nucengdes.2011.01.036.

[6] D. Thomas, F.X. Ouf, F. Gensdarmes, S. Bourrous, L. Bouilloux, Pressure drop model for nanostructured deposits, Sep. Purif. Technol. 138 (2014) 144–152. https://doi.org/10.1016/j.seppur.2014.09.032.

[7] A. Gupta, V.J. Novick, P. Biswas, P.R. Monson, Effect of Humidity and Particle Hygroscopicity on the Mass Loading Capacity of High Efficiency Particulate Air (HEPA) Filters, Aerosol Sci. Technol. 19 (1993) 94–107. https://doi.org/10.1080/02786829308959624.

[8] A. Joubert, J.C. Laborde, L. Bouilloux, S. Chazelet, D. Thomas, Modelling the pressure drop across HEPA filters during cake filtration in the presence of humidity, Chem. Eng. J. 166 (2011) 616–623. https://doi.org/10.1016/j.cej.2010.11.033.

[9] M. Lazghab, K. Saleh, I. Pezron, P. Guigon, L. Komunjer, Wettability assessment of finely divided solids, Powder Technol. 157 (2005) 79–91. https://doi.org/10.1016/j.powtec.2005.05.014.

[10] A.B. Yu, C.L. Feng, R.P. Zou, R.Y. Yang, On the relationship between porosity and interparticle forces, Powder Technol. 130 (2003) 70–76. https://doi.org/10.1016/S0032-5910(02)00228-0.

[11] E.G. Schnitzler, J.M. Gac, W. Jäger, Coating surface tension dependence of soot aggregate restructuring, J. Aerosol Sci. 106 (2017) 43–55. https://doi.org/10.1016/j.jaerosci.2017.01.005.

[12] K. Adachi, S.H. Chung, P.R. Buseck, Shapes of soot aerosol particles and implications

for their effects on climate, J. Geophys. Res. Atmos. 115 (2010). https://doi.org/10.1029/2009JD012868.

[13] Q. Ribeyre, G. Grévillot, A. Charvet, C. Vallières, D. Thomas, Modelling of water adsorption–condensation isotherms on beds of nanoparticles, Chem. Eng. Sci. 113 (2014) 1–10. https://doi.org/10.1016/j.ces.2014.03.027.

[14] F.-X. Ouf, V.-M. Mocho, S. Pontreau, Z. Wang, D. Ferry, J. Yon, Physicochemical properties of aerosol released in the case of a fire involving materials used in the nuclear industry, J. Hazard. Mater. 283 (2015) 340–349. https://doi.org/10.1016/j.jhazmat.2014.09.043.

[15] J. Pastor-Villegas, J.M. Meneses Rodríguez, J.F. Pastor-Valle, J. Rouquerol, R. Denoyel, M. García García, Adsorption-desorption of water vapour on chars prepared from commercial wood charcoals, in relation to their chemical composition, surface chemistry and pore structure, J. Anal. Appl. Pyrolysis. 88 (2010) 124–133. https://doi.org/10.1016/j.jaap.2010.03.005.

[16] J. Choma, M. Jaroniec, Z. Li, J. Klinik, Monitoring Changes in Surface and Structural Properties of Porous Carbons Modified by Different Oxidizing Agents, J. Colloid Interface Sci. 446 (1999) 438–446.

[17] T. Horikawa, T. Muguruma, D.D. Do, K.I. Sotowa, J.R. Alcántara-Avila, Scanning curves of water adsorption on graphitized thermal carbon black and ordered mesoporous carbon, Carbon N. Y. 95 (2015) 137–143. https://doi.org/10.1016/j.carbon.2015.08.034.

[18] A. V. Kiselev, N. V. Kovaleva, Effect of thermal treatment of various carbons on the adsorption of vapors, Bull. Acad. Sci. USSR Div. Chem. Sci. 8 (1959) 955–964. https://doi.org/10.1007/BF00916659.

[19] P.J. Carrott, Adsorption of Water Vapor By Non-Porous Carbons, Carbon N. Y. 30 (1992) 201–205. https://doi.org/10.1097/00010694-195988030-00007.

[20] G. Ferraro, E. Fratini, R. Rausa, P. Fiaschi, P. Baglioni, Multiscale Characterization of Some Commercial Carbon Blacks and Diesel Engine Soot, Energy and Fuels. 30 (2016) 9859–9866. https://doi.org/10.1021/acs.energyfuels.6b01740.

[21] O.B. Popovicheva, N.M. Persiantseva, V. Tishkova, N.K. Shonija, N.A. Zubareva, Quantification of water uptake by soot particles, Environ. Res. Lett. 3 (2008) 025009. https://doi.org/10.1088/1748-9326/3/2/025009.

[22] A.R. Chughtai, G.R. Williams, M.M.O. Atteya, N.J. Miller, D.M. Smith, Carbonaceous particle hydration, Atmos. Environ. 33 (1999) 2679–2687. https://doi.org/10.1016/S1352-2310(98)00329-X.

[23] L. Liu, S. Tan, T. Horikawa, D.D. Do, D. Nicholson, J. Liu, Water adsorption on carbon - A review, Adv. Colloid Interface Sci. 250 (2017) 64–78. https://doi.org/10.1016/j.cis.2017.10.002.

[24] S. Furmaniak, P.A. Gauden, A.P. Terzyk, G. Rychlicki, Water adsorption on carbons - Critical review of the most popular analytical approaches, Adv. Colloid Interface Sci.

137 (2008) 82–143. https://doi.org/10.1016/j.cis.2007.08.001.

[25] M.M.M. Dubinin, E.D.D. Zaverina, V.V. Serpinsky, V. V. Serpinski, The sorption of water vapour by active carbon, J. Chem. Soc. (1955) 1760–1766. https://doi.org/10.1039/JR9550001760.

[26] D. Alibert, M. Coutin, M. Mense, Y. Pizzo, B. Porterie, Effect of oxygen concentration on the combustion of horizontally-oriented slabs of PMMA, Fire Saf. J. 91 (2017) 182–190. https://doi.org/10.1016/j.firesaf.2017.03.051.

[27] S. Bourrous, Q. Ribeyre, L. Lintis, J. Yon, S. Bau, D. Thomas, C. Vallières, F.-X. Ouf, A semi-automatic analysis tool for the determination of primary particle size, overlap coefficient and specific surface area of nanoparticles aggregates., J. Aerosol Sci. 126 (2018) 122–132. https://doi.org/10.1017/S0950268817001236.

[28] K.S.W. Sing, Reporting physisorption data for gas/solid systems with special reference to the determination of surface area and porosity (Recommendations 1984), Pure Appl. Chem. 57 (1985) 603–619. https://doi.org/10.1351/pac198557040603.

[29] P. Parent, C. Laffon, I. Marhaba, D. Ferry, T.Z. Regier, I.K. Ortega, B. Chazallon, Y. Carpentier, C. Focsa, Nanoscale characterization of aircraft soot: a high-resolution transmission electron microscopy, Raman spectroscopy, X-ray photoelectron and near-edge X-ray absorption spectroscopy study, Carbon N. Y. 101 (2016) 86–100. https://doi.org/10.1016/j.carbon.2016.01.040.

[30] F.-X. Ouf, S. Bourrous, S. Fauvel, A. Kort, L. Lintis, J. Nuvoli, J. Yon, True density of combustion emitted particles: A comparison of results highlighting the influence of the organic contents, J. Aerosol Sci. 134 (2019) 1–13. https://doi.org/10.1016/j.jaerosci.2019.04.007.

[31] S.J. Gregg, K.S.W. Sing, Adsorption, surface area and porosity, Second Edi, London, 1982.

[32] K. Miura, Adsorption of Water Vapor from Ambient Atmosphere onto Coal Fines Leading to Spontaneous Heating of Coal Stockpile, Energy and Fuels. 30 (2016) 219–229. https://doi.org/10.1021/acs.energyfuels.5b02324.

[33] H.P. Boehm, Some aspects of the surface chemistry of carbon blacks and other carbons, Carbon N. Y. 32 (1994) 759–769. https://doi.org/10.1016/0008-6223(94)90031-0.

[34] N. Ess, N.P. Ivleva, E.D. Kireeva, F.X. Ouf, R. Niessner, In situ Raman microspectroscopic analysis of soot samples with different OC content : Structural changes during oxidation, Carbon N. Y. 105 (2016) 81377. https://doi.org/10.1016/j.carbon.2016.04.056.

[35] H. Emmett, R.B. Anderson, The Adsorption of Water Vapor on Carbon Black, J. Am. Chem. Soc. 67 (1945) 1492–1494. https://doi.org/10.1021/ja01225a025.

[36] W. Wolf, W.E.L. Spiess, G. Jung, H. Weisser, H. Bizot, R.B. Duckworth, The water-vapour sorption isotherms of microcrystalline cellulose (MCC) and of purified potato starch. Results of a collaborative study, J. Food Eng. 3 (1984) 51–73.

https://doi.org/10.1016/0260-8774(84)90007-4.

[37] P. Arlabosse, E. Rodier, J.H. Ferrasse, S. Chavez, D. Lecomte, Comparison between static and dynamic methods for sorption isotherm measurements, Dry. Technol. 21 (2003) 479–497. https://doi.org/10.1081/DRT-120018458.

[38] Y. Belmabkhout, M. Frère, G. De Weireld, High-pressure adsorption measurements. A comparative study of the volumetric and gravimetric methods, Meas. Sci. Technol. 15 (2004) 848–858. https://doi.org/10.1088/0957-0233/15/5/010.

[39] D. Snoeck, L.F. Velasco, A. Mignon, S. Van Vlierberghe, P. Dubruel, P. Lodewyckx, N. De Belie, The influence of different drying techniques on the water sorption properties of cement-based materials, Cem. Concr. Res. 64 (2014) 54–62. https://doi.org/10.1016/j.cemconres.2014.06.009.

[40] R. Jowitt, P.J. Wagstaffe, The certification of the water content of microcrystalline cellulose at 10 water activities. Commission of the European Communities, reference materials CRM 302., 1989.

[41] C.L. Levoguer, J. Booth, Moisture sorption of EC standard reference material RM 302 on a DVS instrument. DVS Application Note 02., 2014. www.surfacemeasurementsystems.com.

[42] E. Doelker, Comparative compaction properties of various microcrystalline cellulose types and generic products, Drug Dev. Ind. Pharm. 19 (1993) 2399–2471.

[43] R.A. Dobbins, G.W. Mulholland, N.P. Bryner, Comparison of a fractal smoke optics model with light extinction measurements, Atmos. Environ. 28 (1994) 889–897. https://doi.org/10.1016/1352-2310(94)90247-X.

[44] J.S. Newman, J. Steciak, Characterization of particulates from diffusion flames, Combust. Flame. 67 (1987) 55–64. https://doi.org/10.1016/0010-2180(87)90013-7.

[45] G. Prado, J. Jagoda, K. Neoh, J. Lahaye, A study of soot formation in premixed propane/oxygen flames by in-situ optical techniques and sampling probes, Symp. Combust. 18 (1981) 1127–1136. https://doi.org/10.1016/S0082-0784(81)80117-8.

[46] C.M. Megaridis, R.. Dobbins, Morphological Description of Flame-Generated Materials, Combust. Sci. Technol. 71 (1990) 95–109. https://doi.org/10.1080/00102209008951626.

[47] N.P. Levitt, R. Zhang, H. Xue, J. Chen, Heterogeneous Chemistry of Organic Acids on Soot Surfaces, J. Phys. Chem. A. 111 (2007) 4804–4814.

[48] C.J. Liang, J.D. Liao, A.J. Li, C. Chen, H.Y. Lin, X.J. Wang, Y.H. Xu, Relationship between wettabilities and chemical compositions of candle soots, Fuel. 128 (2014) 422–427. https://doi.org/10.1016/j.fuel.2014.03.039.

[49] F. Rouquerol, J. Rouquerol, K.S.W. Sing, P. Lleewellyn, G. Maurin, Adsorption by Powders and Porous Solids, 2nd Editio, Academic Press, Oxford, 2014.

[50] L.F. Velasco, D. Snoeck, A. Mignon, L. Misseeuw, C.O. Ania, S. Van Vlierberghe, P.

Dubruel, N. De Belie, P. Lodewyckx, Role of the surface chemistry of the adsorbent on the initialization step of the water sorption process, Carbon N. Y. 106 (2016) 284–288. https://doi.org/10.1016/j.carbon.2016.05.042.

[51] S. Léonard, G.W. Mulholland, R. Puri, R.J. Santoro, Generation of CO and smoke during underventilated combustion, Combust. Flame. 98 (1994). https://doi.org/10.1016/0010-2180(94)90195-3.

[52] D. Charrière, P. Behra, Water sorption on coals, J. Colloid Interface Sci. 344 (2010) 460–467. https://doi.org/10.1016/j.jcis.2009.11.064.

[53] D.D. Do, Adsorption analysis: equilibria and kinetics, Imperial College Press, London, England, 1998.

[54] M.M. Dubinin, Water vapor adsorption and the microporous structures of carbonaceous adsorbents, Carbon N. Y. 18 (1980) 355–364. https://doi.org/10.1016/0008-6223(80)90007-X.

[55] M.M. Dubinin, V.V. Serpinsky, Isotherm equation for water vapor adsorption by microporous carbonaceous adsorbents, Carbon N. Y. 19 (1981) 402–403.

[56] S.S. Barton, M.J.B. Evans, J.A.F. MacDonald, The Adsorption of Water Vapor by Porous Glass, Carbon N. Y. 29 (1991) 1099–1105.

[57] M.M. Dubinin, G.A. Andreeva, R.S. Vartapetyan, S.P. Vnukov, K.M. Nikolaev, N.S. Polyakov, N.I. Seregina, D.V. Fedoseev, Adsorption of water and the micropore structures of carbon adsorbents, Izv. Akad. Nauk SSSR, Seriya Kim. 11 (1982) 2425–2429.

[58] S. Bourrous, L. Bouilloux, F.-X. Ouf, P. Lemaitre, P. Nerisson, D. Thomas, J.C. Appert-Collin, Measurement and modeling of pressure drop of HEPA filters clogged with ultrafine particles, Powder Technol. 289 (2016). https://doi.org/10.1016/j.powtec.2015.11.020.

Supplementary information I: Table SI-1: TEM illustrations of particles composing soot samples

Samples	TEM illustration	TEM illustration
Soot		
Heptane (lab scale) • Left : 21 % [O2] • Right : 15 % [O2]	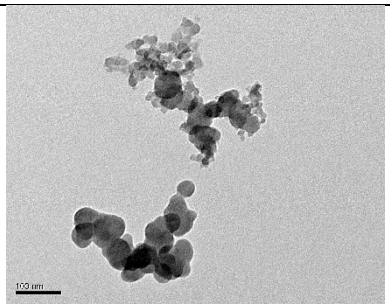	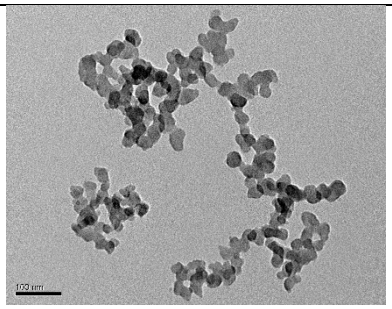
PMMA (lab scale) • Left : 21 % [O2] • Right : 18 % [O2]	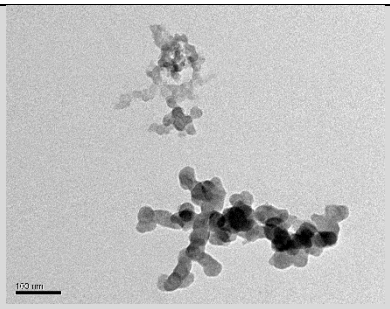	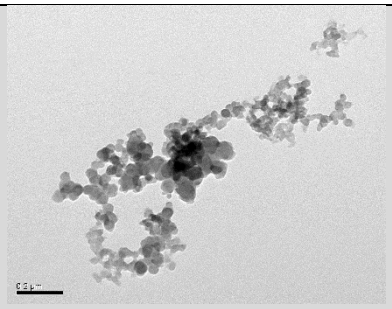
DTE Medium oil (lab scale) • Left : 21 % [O2] • Right : 18 % [O2]	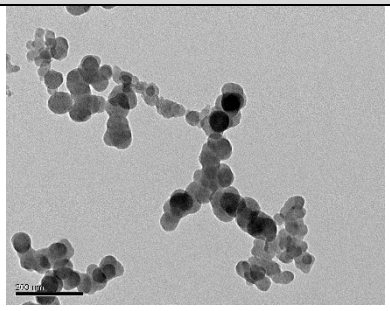	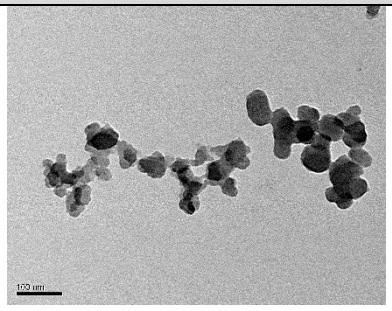
Heptane (pilot scale) • Left : 21 % [O2] • Right : 15 % [O2]	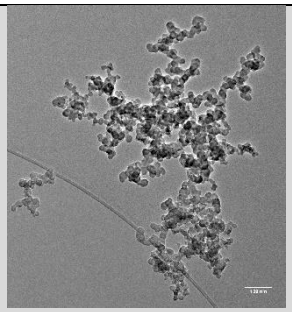	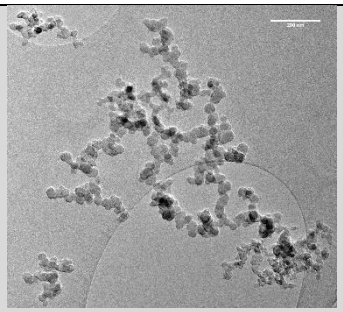
PMMA (pilot scale) • Left : 21 % [O2] • Right : 18 % [O2]	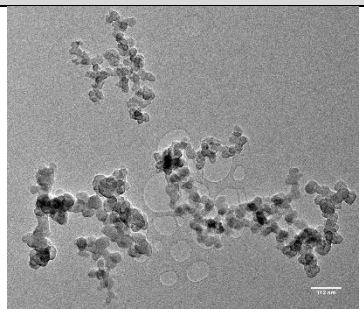	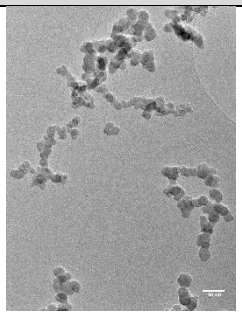

Supplementary information I: Table SI-2: TEM illustrations of particles composing carbon blacks samples

Samples	TEM illustration
Carbon blacks	
PRINTEX 90	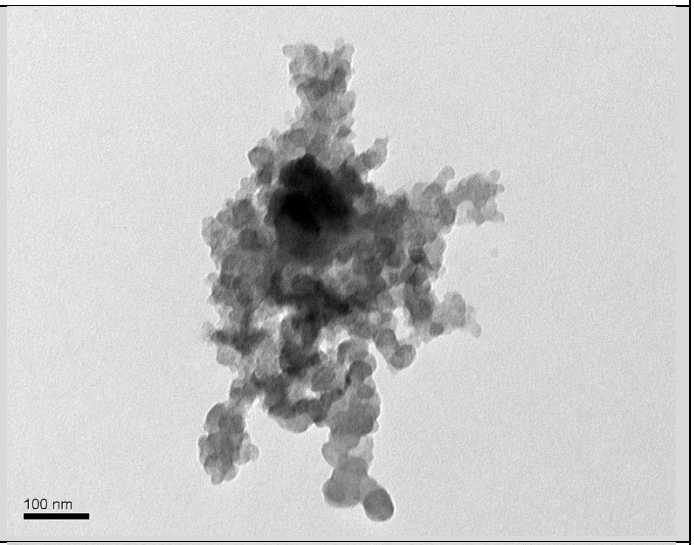
FLAMMRUS 101	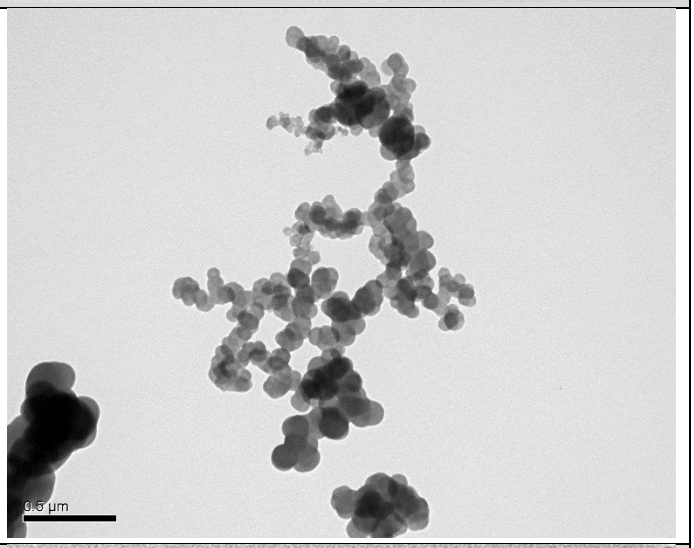
COLOUR BLACK FW200	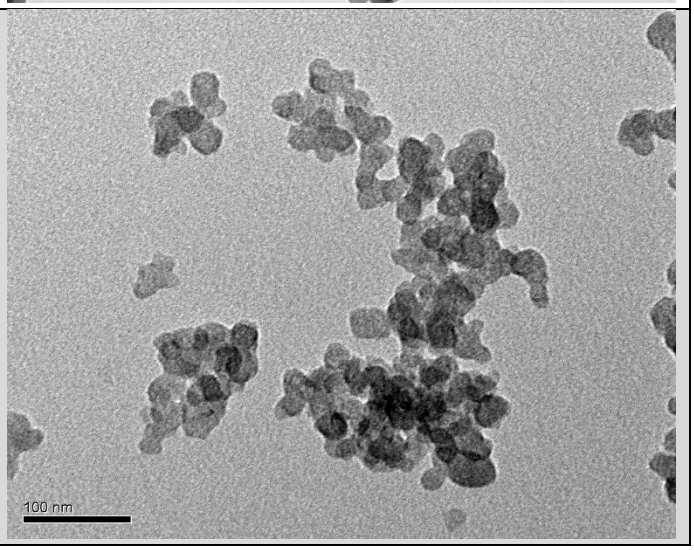

Supplementary information II: oxygen depletion effect on water uptake

Fig. SII-1 presents the evolution, as a function of dioxygen concentration, of the dimensionless water uptake, defined as ratio between water uptake at considered oxygen concentration and water uptake at dioxygen concentration of 21%. One must notice that this ratio has been computed for the maximum water uptake, i.e. for a relative humidity of 90%.

$$Dimensionless\ water\ uptake\ (RH) = \frac{a_{[O_2]}(RH)}{a_{[O_2]=21\%}(RH)} \qquad \text{(Eq. S-1)}$$

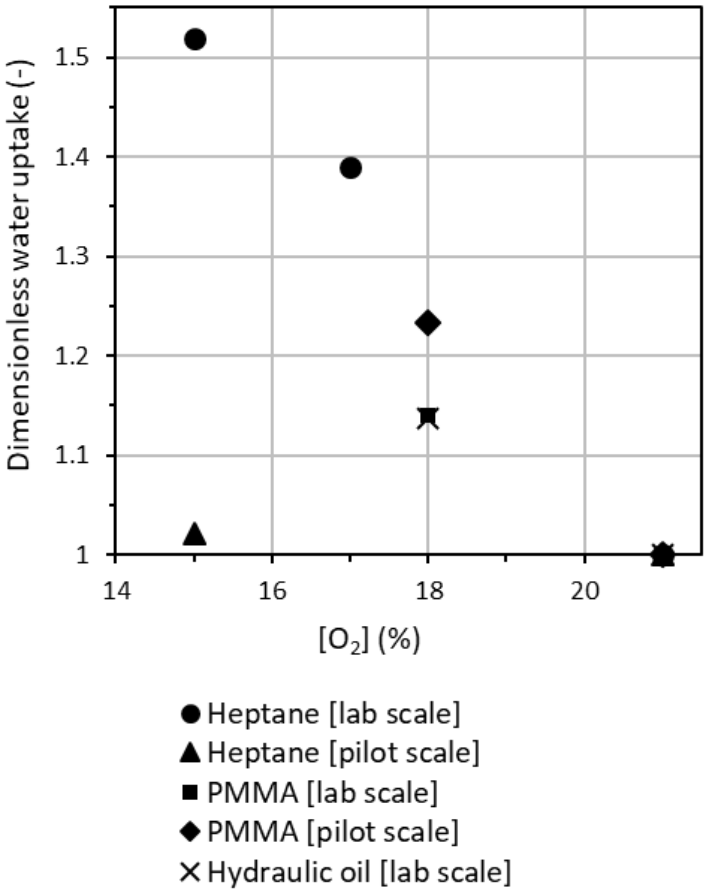

Figure SI-1: Evolution of dimensionless water uptake as a function of dioxygen concentration

Supplementary information III: water isotherms for carbon black samples

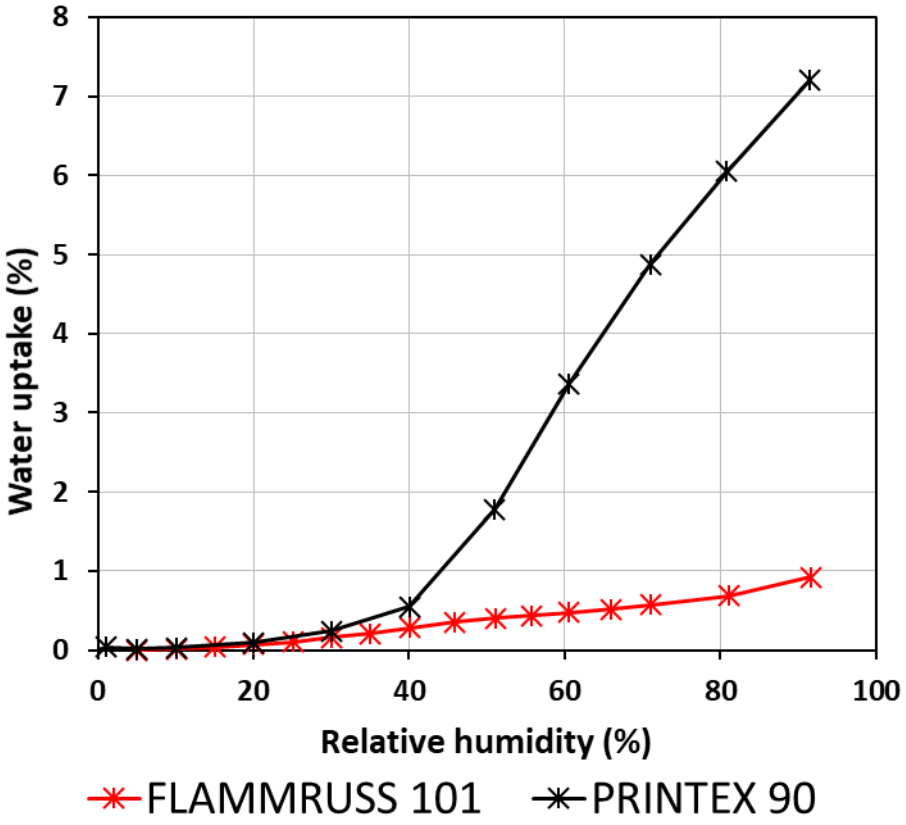

Figure SI-2: water adsorption isotherms for Flammruss 101 and Printex 90

664 **Supplementary information IV: water isotherms obtained for samples in powder forms**

665

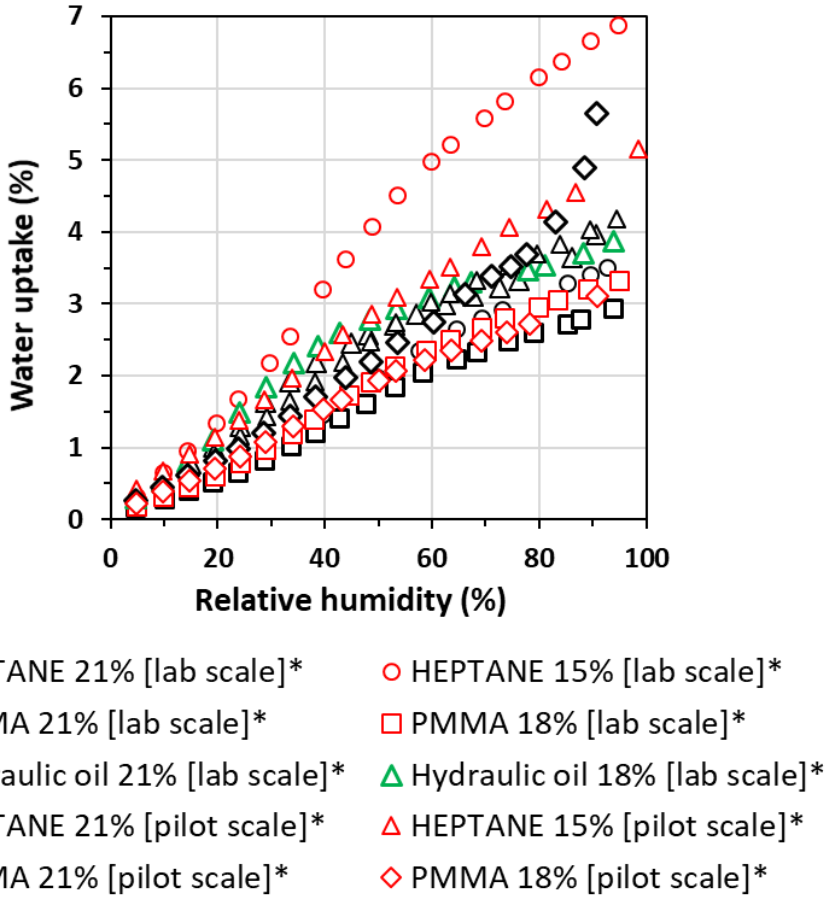

666

667 Figure SI-3: Water adsorption isotherms obtained for samples in powder forms

668

669

Supplementary information V: DS2 fitting of experimental water adsorption isotherms

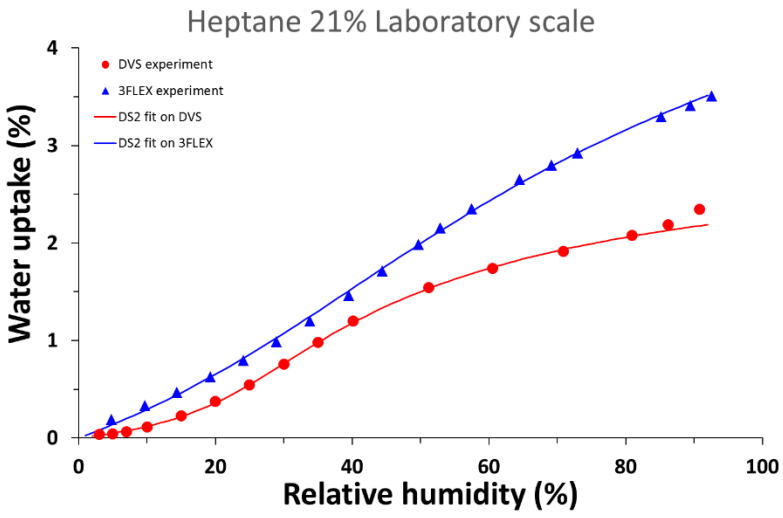

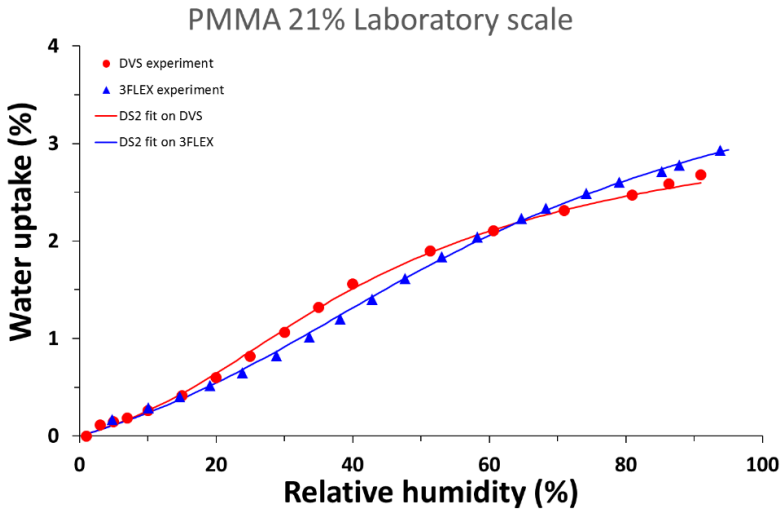

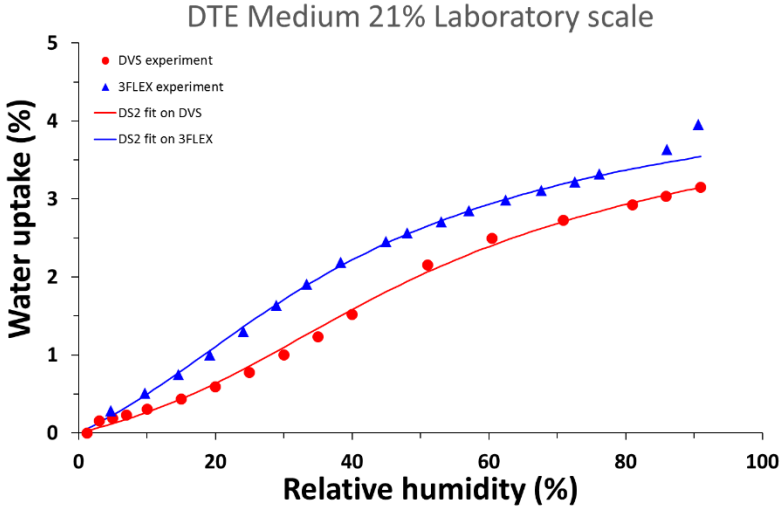

Figure SI-4: DS2 fitting of experimental water adsorption isotherms

Supplementary information VI: Table SI-3: Summary of DS2 model's constants of studied soot samples

Samples	Pellet form					Powder form				
	ε_{pellet} (%)	k (%)	a_0 $(\%g.g_{ads.}^{-1})$	c (-)	R^2	ε_{powder} (%)	k (%)	a_0 $(\%g.g_{ads.}^{-1})$	c (-)	R^2
Heptane 21% (lab scale)	62±3	0.323	0.254	3.317	0.999	96 ± 1	0.149	1.688	1.542	0.999
Heptane 15% (lab scale)	54±4	0.242	0.554	3.185	0.997		0.088	2.807	1.884	1.000
PMMA 21% (lab scale)	54±4	0.269	0.711	2.864	0.999		0.197	1.153	1.797	0.999
PMMA 18% (lab scale)	29±7	0.209	1.069	2.242	0.999		0.177	1.354	1.823	0.999
DTE Medium oil 21% (lab scale)	58±10	0.200	0.962	2.276	0.996		0.200	1.632	2.593	0.999
DTE Medium oil 18% (lab scale)	56±10	0.191	1.709	2.297	0.998		0.206	1.246	3.339	0.999
Heptane 21% (pilot scale)	66±3	0.213	1.805	1.876	0.998		0.127	3.822	1.174	0.999
Heptane 15% (pilot scale)	58±4	0.229	1.395	2.825	0.998		0.059	28.323	0.221	0.999
PMMA 21% (pilot scale)	59±4	0.290	0.510	3.143	0.999		0.021	12.910	0.313	0.999
PMMA 18% (pilot scale)	52±4	0.235	1.211	2.801	0.999		0.191	2.170	1.481	0.999
average values	55±10	0.24 ± 0.02	1.0 ± 0.4	2.6 ± 0.4	-	96±1	0.14 ± 0.03	2.6 ± 0.4	1.6 ± 0.4	-